Received: 6 June 2024 | Revised: 10 August 2024 | Accepted: 17 September 2024

IET Electric Power Applications

DOI: 10.1049/elp2.12504

ORIGINAL RESEARCH

Modelling and optimization of TPMLMs with slotted stators based on Bayesian DNN

Tao Wu[1,2,3] | Peipei Dai[1,2,3] | Kai Zhu[1,2,3] | Yachao Zhu[4]

[1]School of Automation, China University of Geosciences, Wuhan, China

[2]Hubei Key Laboratory of Advanced Control and Intelligent Automation for Complex Systems, Wuhan, China

[3]Engineering Research Center of Intelligent Technology for Geo-Exploration, Ministry of Education, Wuhan, China

[4]School of Electrical and Data Engineering, University of Technology Sydney, Ultimo, New South Wales, Australia

Correspondence

Yachao Zhu.
Email: yachao.zhu@uts.edu.au

Funding information

National Natural Science Foundation of China, Grant/Award Number: 2021343163

Abstract

The Permanent Magnet Linear Motor (TPMLM) is widely used in different industrial fields. TPMLMs with slots and iron cores have high power density, but their thrust fluctuations and copper losses are significant. Due to the nonlinearity and saturation of magnetic circuits, their electromagnetic models are complex and the accuracy of numerical methods is very inferior. Substantially accurate modelling is crucial for motor optimisation design. In this paper, a data-driven modelling method based on Bayesian optimisation deep neural network (DNN) is proposed to improve the accuracy of the electromagnetic field. The finite element (FE) modelling under different structural parameters is analysed and provides a training dataset for DNN. Then, a multi-objective optimisation problem for the slotted TPMLM is carried out based on the multi-objective black hole algorithm. Compared to the original design, the average thrust of TPMLM increased by 49.37%, the thrust fluctuation percentage decreased by 9.59%, and the coil copper consumption percentage decreased by 2.64%. The results show that the improved DNN model has very high modelling accuracy, providing a new way for motor design and optimisation.

KEYWORDS

learning (artificial intelligence), neural nets, optimisation, permanent magnet motors

1 | INTRODUCTION

Tubular Permanent Magnet Linear Motors (TPMLMs) are renowned for their ease of installation, compact size, absence of transverse edge effects, and high thrust density. These characteristics make them well-suited for various cylindrical applications such as chillers [1], machine tool spindle drives [2], and subsea drilling impactors. However, as drilling depths increase, the performance requirements for TPMLMs, which serve as the power penetration device for new electromagnetic impactors, also escalate. Traditional TPMLMs with slottedless and coreless structures often struggle with insufficient power density and excitation force, decreasing drilling speeds after the sampler drills into deeper depths [3]. Therefore, the research focus of global studies has shifted to the optimal design of slotted TPMLM with greater thrust density at the same speed [4].

In practice, slotted TPMLMs often face the problem of large thrust fluctuations. In high-speed, short-stroke applications, the coils of TPMLMs are prone to heat up and cause local overheating, and eddy-current loss concentration becomes large, which can lead to irreversible demagnetisation of permanent magnets in prolonged operation. Such conditions severely impact the motor's performance and life [5]. To enhance the motor's comprehensive performance, there is a critical need for an accurate and efficient electromagnetic calculation model, which is essential for its optimal design [6].

The traditional electromagnetic field modelling and analysis methods for motors are mainly Finite Element Analysis (FEA), Equivalent Magnetic Circuit (EMC) and Electromagnetic Analysis. Due to their structural complexity, TPMLMs with slots and cores face many challenges in modelling and analysis. While FEA can provide high computational accuracy, its computational process is cumbersome and time-consuming

[7]. It requires many iterative calculations, dramatically increasing the amount of computation and appearing remarkably inefficient for multi-objective optimization design calculations. EMC is limited to qualitative analysis and lacks the precision necessary for detailed design optimization [8]. Electromagnetic analytical models, though capable of quantitative analysis, often fail to accurately capture the nonlinear characteristics and magnetic field distribution inside the motor due to their simplifying assumptions, resulting in poor accuracy [9]. Therefore, traditional modelling and optimization methods are challenging in meeting the current demand for efficient and high-precision TPMLM design, and there is an urgent need to explore new modelling and optimization strategies [10].

To address these limitations, data-driven modelling methods, such as Random Forest (RF) [11], Support Vector Machine (SVM) [12], and Deep Neural Network (DNN) [13], have emerged as promising solutions for electromagnetic mechanism modelling in TPMLMs. These methods aim to fit the real data mapping relationship based on the input and output data of the analysis object.

Design optimisation becomes a crucial step after constructing an electromagnetic model for TPMLMs. The optimal design objective for slotted TPMLMs is to maximise shock work and efficiency within the constraints of limited motor size and space while also minimising the amount of permanent magnets used [14]. This presents a constrained, multi-objective, multi-variable, and complex nonlinear optimization problem [15]. A specific analysis is required to define the multi-objective optimization model of the motor, with the objective function and constraints clearly described by mathematical expressions. Commonly used multi-objective evolutionary algorithms are as follows: Multi-objective particle swarm optimization [16], nondominated sorting genetic algorithm II (NSGA-II) [17] , multi-objective evolutionary algorithm based on decomposition [18] and Multi-objective Black Hole Algorithm [19] (AMOBH).Is it possible to combine the data-driven modelling of the electromagnetic field with the objective function to achieve the multi-objective optimization of TPMLM?

A deep neural network modelling approach based on Bayesian optimization is proposed to build a data-driven model of the TPMLM from its electromagnetic field finite element model. Then, the multi-objective black hole algorithm is used to perform multi-objective optimization of the electromagnetic performance of TPMLM. Comparative experimental results show that the method significantly improves performance.

This paper has three main contributions:

1) A finite element model of TPMLM is established based on structural parameters and electromagnetism.
2) A data-driven modelling method based on DNN is proposed to solve the problem of low computational efficiency of traditional mechanical models.
3) A multi-objective optimization method based on the multi-objective black hole algorithm for cylindrical permanent magnet linear motors is proposed, significantly improves the thrust performance of the TPMLM while effectively reducing the percentage of coil copper consumption.

2 | MOTOR STRUCTURE AND FINITE ELEMENT ANALYSIS

2.1 | Motor structure

The schematic structure of the TPMLM is shown in Figure 1, which is a moving-iron linear motor consisting of three parts: the mover, the air gap and the stator. The mover includes permanent magnets, pole shoes and secondary cores. The stator contains primary cores and three-phase AC windings [20]. The permanent magnets are magnetised axially along the z-axis, and the three regions marked by the blue line in the figure are divided according to the differences in the magnetic permeability of the various parts of the motor. The main parameters of the TPMLM are shown in Table 1.

2.2 | Finite element analysis method

The magnetic field resolution is often complicated for permanent magnet motors with slots and cores. To simplify the calculation, according to the symmetry of the TPMLM, the z-axis of the cylindrical permanent magnet synchronous motor can be regarded as the axis of symmetry. The two-dimensional axisymmetric finite element analysis model can be established and simulated using Ansys Maxwell software in the cylindrical coordinate system.

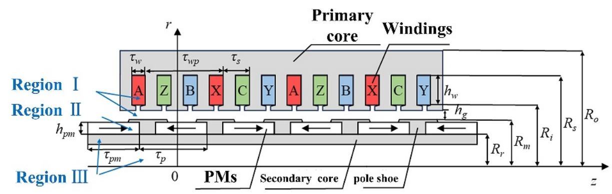

FIGURE 1 Parametric structure diagram of TPMLM.

TABLE 1 Main parts dimensional parameters of the TPMLM.

Quantity	Symbol	Value	Unit
Inner radius of PM	R_r	8.5	mm
Outer radius of mover	R_m	15.9	mm
Inner radius of stator	R_i	17.9	mm
Outer radius of stator	R_s	25.9	mm
Outer radius of motor	R_o	33.4	mm
Air gap length	g	1	mm
Pole pitch	τ_p	36	mm
Stator slot pitch	τ_s	12	mm
Axial length of PM	τ_{pm}	18	mm
Thickness of PM	h_{pm}	6	mm
Slot opening width	B_{s0}	2	mm
Thickness of the air gap	h_g	0.7	mm
Radial width of the coil	h_{coil}	8	mm

The following steps are followed for the finite element analysis of the electromagnetic field of the TPMLM:

1) Construct the geometrical model and set up the solution domain, the geometrical model of slotted TPMLM finite element analysis established in Figure 2.
2) Select suitable materials for different parts of the motor. The specific parameters of the materials are shown in Table 2.
3) Setting the boundary conditions and applying the winding excitation, a pole-slot combination of 10 poles and 12 slots is used in this model to keep the primary and secondary lengths constant. The winding excitation is a three-phase AC current excitation with a current frequency of 50 Hz, and the RMS values of the currents are set according to (1), where J_m is the current density, and S_d is the cross-sectional area of the enamelled wire.

$$i = J_m S_d \tag{1}$$

4) Grid division for the solution domain: set the linear motion range of the actuator, the movement time.
5) View the post-processing results and perform simulation analysis. After setting the relevant parameters, the changes in the motor structure are simulated by changing the values of several parameters(X). The average thrust, thrust fluctuation, and average copper loss of the motor are recorded while keeping other conditions constant, and a total of 1440 simulation sets are generated. Figure 3 illustrates the magnetic field cloud for the motor in its default position at the initial time. Figure 4 shows the transient thrust waveforms when running for one electrical cycle (twice the pole pitch) by varying the slot opening width B_{s0} of the TPMLM with all other conditions constant. The dotted line's left side is the distribution of magnetic force lines, and the right side is the distribution of magnetic induction intensity. Table 3 shows the 1440 sets of data generated by the FEA.

$$\boldsymbol{X} = \left[B_{s0}, \tau_{pm}, h_g, h_{coil}, h_{pm}\right] \tag{2}$$

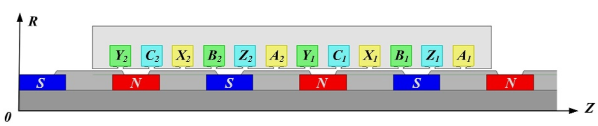

FIGURE 2 Geometrical model diagram for FEA of TPMLM.

3 | DATA-DRIVEN MODEL BASED ON OPTIMIZED DNN

3.1 | Model structure of deep neural network

The Deep Neural Network (DNN) is a type of deep learning model that builds a multilayer network structure. It autonomously learns features of input data through optimization algorithms, such as gradient descent to solve the problems of classification, recognition, regression, etc. The design of DNN needs to consider the layer structure of the neural network, activation function, optimization algorithm, loss function and other elements, which can improve its prediction performance according to the dataset used [21]. The design of DNN needs to consider the layer structure of the neural network, activation function, optimization algorithm, loss function and other elements, according to the dataset used to build a DNN model reasonably can improve its prediction performance.

A DNN usually consists of an input layer, multiple hidden layers, and an output layer. It includes numerous neurons, with each neuron in a layer connecting to all neurons in the preceding layer, each connection characterised by a weight. The neuron is the basic unit of DNN, and its basic structure is shown in Figure 5. The circle in the figure represents the current neuron, where x_i represents the input from the ith neuron in the previous layer, ω_i is the connection weight of the i th neuron, and θ represents the output threshold, also known as the bias term.

A neural network is formed by connecting several of the above neurons in a layer-to-layer fashion.

When the weighted value of the input is less than the threshold, neurons will use different activation functions to output the nonlinear relationship related to the input, and the output y can be expressed by the following formula:

$$y = f\left\{\sum_{i=1}^{n} (\omega_i x_i - \theta)\right\} \tag{3}$$

Where $\omega_i x_i$ is the input weighted value and f is the nonlinear activation function. With the introduction of a nonlinear activation function, DNN can fit high-dimensional complex nonlinear relations. Figure 6 illustrates four common activation functions. Different activation functions can completely change the training speed and prediction performance of the model.

TABLE 2 Material-specific parameters.

No.	Areas	Materials	Relative permeability	Conductivity
1	Pri- core, pole shoe	DW310-50	B-H curve	0
2	Seco- core	Steel-stainless	1	1,100,000 s/m
3	PMs	NdFe35	1.09978	625,000 s/m
4	Coil	Copper	0.99999	58,000,000
5	Vacuums	Vacuum	1	0

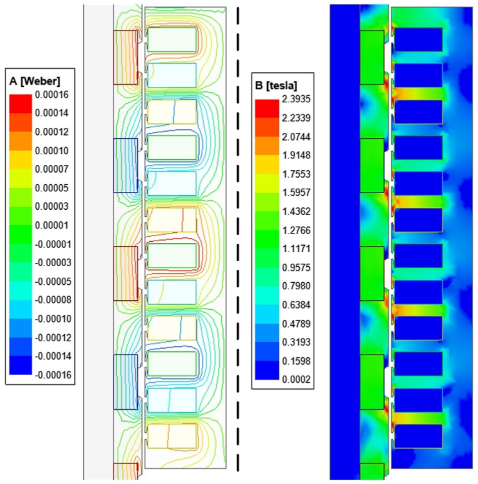

FIGURE 3 Motor magnetic field cloud at initial position.

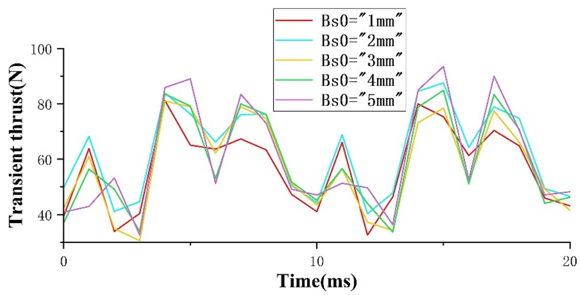

FIGURE 4 Transient thrust waveform of FEA.

TABLE 3 Data set of FEA.

No.	Parametric variable X/mm	F_{av}/N	F_{pk}/N	P_{cua}/W
1	[2 , 18 , 0.7 , 8 , 4.8]	57.10	29.81	17.15
2	[3 , 18 , 0.7 , 8 , 4.8]	54.66	44.80	17.15
3	[2 , 18 , 0.7 , 9 , 4.8]	63.92	32.64	19.72
…	……	…	…	…
822	[2.8 , 21.6 , 1.3 , 8 , 4.8]	69.79	25.26	17.67
823	[2.2 , 21.6 , 1.3 , 9 , 4.8]	67.48	17.86	20.30
824	[2.5 , 21.6 , 1.3 , 9 , 4.8]	64.90	19.02	20.30
…	……	…	…	…
1438	[2.2 , 28.8 , 1.3 , 10 , 6.8]	121.42	66.85	25.18
1439	[2.5 , 28.8 , 1.3 , 10 , 6.8]	125.70	65.15	25.18
1440	[2.8 , 28.8 , 1.3 , 10 , 6.8]	115.95	66.23	25.18

Optimization algorithms are a key part of the neural network training process, which is used to select the best-fitting combination of model parameters by iteratively updating the neural network's weights and intercept-minimising loss function.

In this paper, DNN models are used to fit high-dimensional nonlinear relationships between different motor parameters and the output performance parameters, which is essentially a regression problem. For regression problems, the objective function of DNN is often chosen as Mean Squared Error (MSE) to measure the difference between the predicted and actual values of the model. For a dataset with one sample, the MSE is defined as follows:

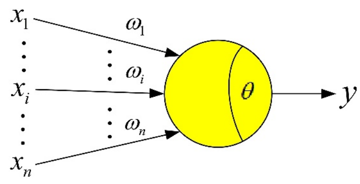

FIGURE 5 Structure of neurons.

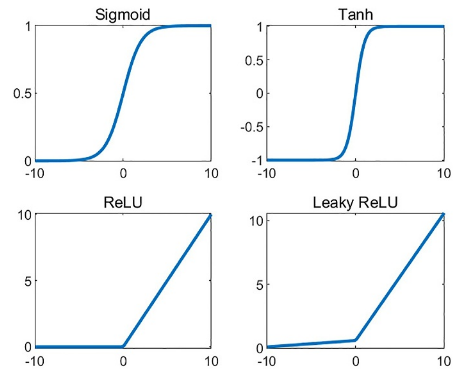

FIGURE 6 Common activation functions.

$$MSE = \frac{1}{n}\sum_{i=1}^{n}\left(y_i - \hat{y}_i\right)^2 \tag{4}$$

3.2 | Bayesian optimised DNN model

Parameters that need to be set manually in DNNs are called hyperparameters. Unlike the weights and biases of the model, hyperparameters cannot be learnt from training data and must be optimised through experimentation and search to find the best values.

Hyperparameter optimization is the process of improving the model performance and generalisation ability by adjusting the hyperparameters in the neural network model. The goal is to find an optimal set of hyperparameter configurations that enable the trained model performance well on the validation and test sets.

Determining the optimal hyperparameter combination with traditional grid search and random search methods is often difficult. Bayesian optimization is a global optimization method based on Bayes' theorem, which finds the global optimal solution in as few iterations as possible by choosing the next sampling point in an unknown region of the objective function and updating the estimate of the objective function. The general process of Bayesian optimization of hyperparameters is shown in Figure 7.

Firstly, the FEA data obtained in the previous chapter was subjected to data preprocessing, including data normalisation, outlier detection, and feature selection on the dataset using the L1 regularisation method. L1 regularisation induces the sparsification of features by making the weights of certain features in the model zero. By sparsifying the feature weights, the L1 regularisation term can exclude features that do not contribute to the prediction task, improving the generalisation ability and interpretability of the model. For DNN, the loss function after adding L1 regularisation can be expressed as:

$$J(\theta) = Loss(\theta) + \lambda \sum_{i=1}^{n} |\theta_i| \tag{5}$$

Where $J(\theta)$ is the total loss function after adding the L1 regularisation term, Loss(θ) is the initial loss function, λ is the regularisation parameter, which is used to control the strength of regularisation, and θ_i represents the ith parameter.

These pre-processing steps can improve the data quality and avoid the interference of the data on the subsequent analyses to speed up the training speed of the model and reduce the number of algorithm iterations and computation time.

Then, the pre-processed data are divided into training, validation and test set according to 8:1:1.

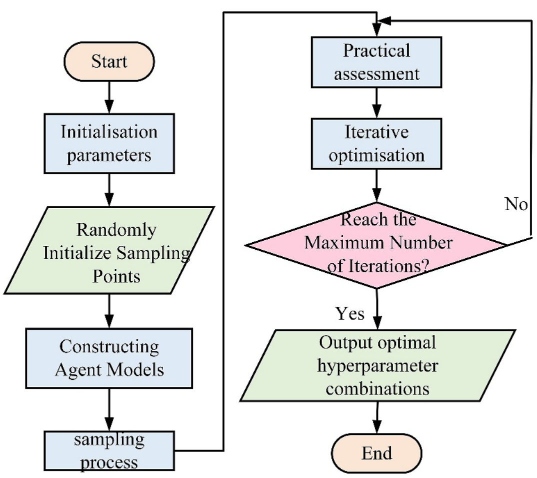

FIGURE 7 General process for Bayesian optimization of hyperparameters.

Next, according to the optimization process, the Bayesian optimization algorithm is used to optimise the hyperparameters of the DNN, and the maximum number of iterations of the algorithm is equal to 6. The hyperparameters to be optimised are the activation function, the optimization algorithm, the number of hidden layers, the number of neurons in each hidden layer, the penalty coefficient of the L1 regularity term and the initial learning rate, and the specific hyperparameter settings are shown in Table 4.

It is worth noting that, compared to algorithms such as gradient descent, L-BFGS automatically adjusts the step size by approximating the Hessian matrix, making manual setting of the learning rate unnecessary.

Additionally, the initial sampling points for hyperparameters are set as follows: the activation function is ReLU, the optimization algorithm is Adam, the number of hidden layers is 3, the number of neurons in each layer is 10, the L1 regularisation penalty coefficient is 0.0001, and the initial learning rate is 0.001.

Finally, after reaching the maximum number of iterations, the optimization process is halted, and the best hyperparameters are output. This is used to train the DNN model one last time. The model's predictive performance is obtained by evaluating the metrics on the test set.

3.3 | Evaluation of Bayesian-DNN model

To validate the accuracy of the DNN model, the root mean square error (RMSE), mean absolute error (MAE) and correlation coefficient (R^2) are selected as the evaluation metrics for model training accuracy and generalisation performance. As the model in this chapter is a multi-input and multi-output model, these three assessment indicators were modified from the original based on the model characteristics.

$$\mathrm{RMSE} = \sqrt{\frac{1}{nm}\sum_{i=1}^{n} \sum_{j=1}^{m} \left(y_{ij} - \hat{y}_{ij}\right)^2} \tag{6}$$

MAE is used to measure the unbiasedness of a model, as it can avoid the mutual offset of errors and accurately reflect the actual prediction error. Its calculation formula is as follows:

$$\mathrm{MAE} = \frac{1}{nm}\sum_{i=1}^{n} \sum_{j=1}^{m} |y_{ij} - \hat{y}_{ij}| \tag{7}$$

TABLE 4 Setting of hyperparameters to be optimised by DNN.

No.	Hyperparameterisation	Range
1	Activation function	[Sigmoid, Tanh, ReLU]
2	Optimization algorithm	[Adam, SGD, RMSprop, L-BFGS]
3	Number of hidden layers	1~5
4	Number of neurons in each hidden layer	0~300
5	L1 regular term penalty factor	10^{-6}~10^{-2}
6	Initial learning rate	10^{-6}~10^{-2}

R2 is used to evaluate the fitting degree of the model to the true values, and its calculation formula is:

$$R^2 = 1 - \frac{\sum_{i=1}^{n} \sum_{j=1}^{m} \left(y_{ij} - \hat{y}_{ij}\right)^2}{\sum_{i=1}^{n} \sum_{j=1}^{m} \left(y_{ij} - y_{ij}\right)^2} \quad (8)$$

In (6), (7) and (8), n represents the number of samples for the motor thermal field, m is the number of labels, $\hat{y}_{ij}$ is the predicted value of the jth label of the ith sample, y_{ij} is the true value of the jth label of the ith sample, and $\overline{y}_j$ is the mean value of the jth label.

3.4 | Prediction results and analysis

Firstly, the dataset was sequentially normalised and 3-Sigma outlier detection was performed, and the results are shown in Figure 8, where the horizontal coordinates represent the number of different columns of the dataset, the first five columns are the features and the last three columns are the labels, the vertical coordinates are the true values of the data after normalisation.

Twenty-one sets of abnormal data are removed. The remaining 749 datasets were divided into training, validation, and test sets in an 8:1:1 ratio. In addition, the maximum training period of the DNN was set to 70, the batch sample size was 50, and the learning rate was automatically updated during training using a linear decay function with a decay coefficient of 0.2 and a decay period of 10 epochs.

Figure 9 illustrates the number of iterations-minimum objective value plot of the objective function of the Bayesian algorithm for DNN hyper-parameter optimization, where the blue line represents the minimum observed value (the value of the loss function obtained on the validation set) in each iteration. The green line represents the minimum estimated value of the Gaussian process agent model on the loss function of the DNN.

From the curves, it can be seen intuitively that in the whole iteration process, the observed value and the estimated value are very close to each other, indicating that the loss of DNN can be accurately fitted by using the Gaussian process agent model. From the third iteration onwards, both curves stabilise, indicating that the algorithm has converged. The final target observation value is 0.00534, with an optimization time of about 5 min.

The optimised DNN hyperparameters are set as follows: the number of hidden layers is 3, the number of neurons in the hidden layer is 30, 21 and 15 respectively; the activation function is selected as ReLU, the optimization algorithm is Adam, and the initial learning rate is 0.0028.

Similarly, the RF and SVM models also use Bayesian algorithm to optimise the hyperparameters, and the parameters of each model are finally set as follows: the number of trees in RF is set to 299, the minimum number of samples of leaf nodes of each tree is set to 1, and the number of features used for segmentation in each tree is set to 4; the weight of the slack

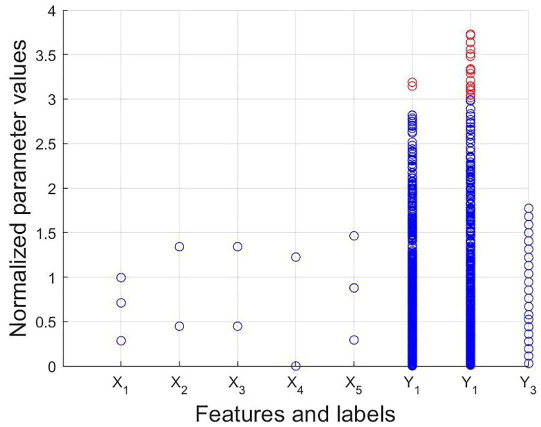

FIGURE 8 Outlier detection results for FEA data.

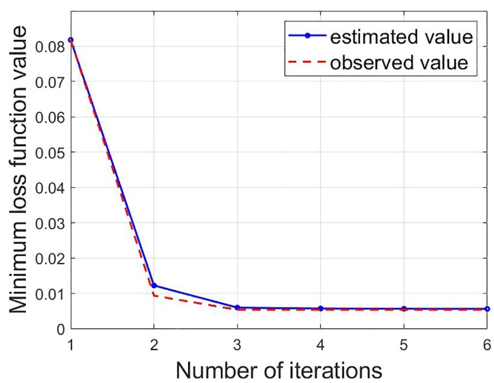

FIGURE 9 Objective function iteration-minimum value curve.

variables of each observation in SVM is set to 0.13644, and the kernel function is chosen to be the Gaussian kernel function RBF, and the width of the kernel function is 0.20078; After determining the hyperparameters of each model, the prediction results of the three models on average thrust, thrust fluctuation and coil copper consumption were obtained through training, and the comparison of these results with the real data in the test set is shown in Figures 10–12.

At the same time, a conventional electromagnetic (EM) analysis model is introduced to generate the corresponding 1440 sets of results when the input parameters are the same. To demonstrate the superiority of the DNN model more intuitively and quantitatively, the evaluation metrics of each data-driven model and the EM parsing method on the same test set are separately derived using ten-fold cross-validation, and the results are shown in Table 5.

From Table 6 reveals that with sufficient FEA training samples:

1) The RMSE, MAE, and R2 of the RF model are slightly better than those of the SVM model, the possible reason being that the SVM may have limited performance when dealing with high dimensional and non-linear data, while the RF is an integrated model based on decision trees, which have a natural ability to model non-linearities.

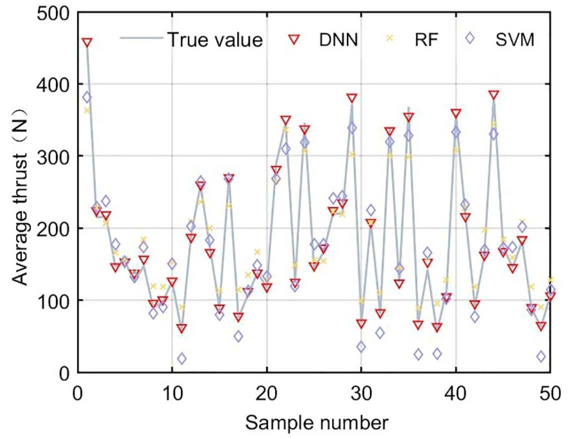

FIGURE 10 Comparison of average thrust prediction results.

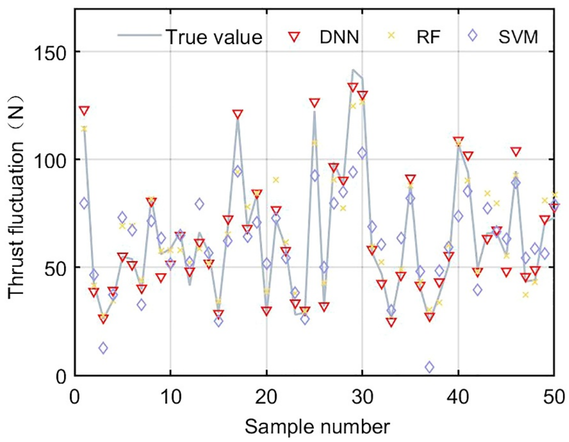

FIGURE 11 Comparison of Thrust fluctuation prediction results.

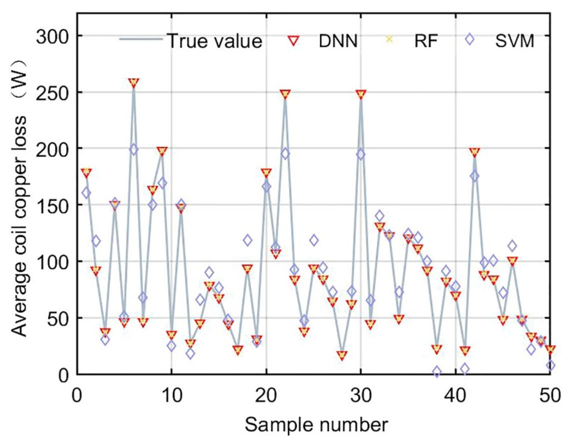

FIGURE 12 Comparison of Coil copper loss predictions results.

2) The RMSE, MAE, and R2 of the DNN model are better than those of the RF and SVM models because DNN learns the abstract features of the data level by level through multiple hidden layers, which enables the network to understand the hierarchical structure of the data better.

TABLE 5 Comparison of the metrics of the models.

	MAE	RMSE	R^2
DNN	**1.568**	**2.276**	**0.9948**
RF	2.607	4.269	0.9375
SVM	2.965	4.833	0.9190
EM model	5.139	7.088	0.6865

TABLE 6 Comparison of significant influence results of different variables.

Variable	Unit	F_{av} (N)	F_{pk} (N)	P_{cua} (W)
J_m	A/mm^2	Outstanding	Outstanding	Outstanding
h_g	mm	**NO**	Outstanding	**NO**
h_w	mm	Outstanding	Outstanding	Outstanding
h_{pm}	mm	Outstanding	Outstanding	Outstanding
τ_w	mm	Outstanding	**NO**	Outstanding
τ_{pm}	mm	**NO**	Outstanding	**NO**

3) The RMSE, MAE, and R2 of the three data-driven models are better than those of the EM mechanism model, which verifies the validity and superiority of the data-driven models in the finite element sample set.

The results show that the DNN model optimised with the Bayesian optimization algorithm exhibits excellent performance when dealing with the fitting task of the TPMLM dataset. In addition, how to effectively apply the established data model to the actual optimization process of TPMLM becomes a key issue that needs to be solved.

4 | OPTIMIZATION AND COMPARISON

4.1 | Analysis of multi-objective optimal design

The main optimization objective of the motor studied in this paper, which is applied to an impactor in a subsea drilling system, is to overcome the disadvantage of the lack of power of the slottedless coreless motor, which needs to ensure that the average thrust is sufficiently high. Secondly, due to the high downhole temperatures and poor cooling conditions, the coil copper consumption needs to be minimised. In addition, the thrust fluctuations of slotted TPMLMs are usually much larger than those of slottedless motors, so they also need to be minimised as much as possible. The three practical requirements mentioned above are competing and contradictory, which is a multi-objective optimization problem that needs to be solved by optimising the motor parameters, and the mathematical model of the multi-objective objective function and its constraints are defined in this section as follows:

$$\min: \quad f_1(x) = \frac{C_f}{F_{av}}$$

$$f_2(x) = C_f P_{cua}\%$$

$$f_3(x) = C_f F_{pk}$$

$$s.t. \quad g_1(x) = F_{av} \geq 100 \text{ N} \tag{9}$$

$$g_2(x) = \frac{F_{pk}}{F_{av}} \in (0, 0.25)$$

$$g_3(x) = P_{cua} \leq 50 \text{ W}$$

$$g_4(x) = V_{pm} \leq 30000 \text{ mm}^3$$

Where the objective function represents the maximisation of average thrust, minimisation of thrust fluctuation and minimisation of coil copper consumption percentage, and the constraints limit the range of average thrust, coil copper consumption percentage, thrust fluctuation percentage and the volume of individual permanent magnets, respectively. One is the penalty factor, which is 100 when the solution does not satisfy the constraints and defaults to C_f. Percentage coil copper consumption $P_{cua}\%$ denotes the ratio of coil copper consumption to the total output power of the motor as follows:

$$P_{cua}\% = \frac{P_{cua}}{P_{cua} + F_{av}v_N} \tag{10}$$

The v_N is the rated linear speed of the motor, calculated in (11). In addition, the volume of a single PM is calculated in (12). R_r is the inner diameter of the permanent magnet.

$$V_s = 2f\tau_p \tag{11}$$

$$V_{pm} = 2\pi\left(\left(R_r + h_{pm}\right)^2 - {R_r}^2\right) \times \tau_{pm} \tag{12}$$

To achieve a better multi-objective optimization effect, it is necessary to study the degree of influence of different motor parameters on the objective function, which will provide an important reference basis for the selection of the variables to be optimised, and then based on the modelling methods proposed in the previous chapter to establish a more accurate approximation model. The combination of orthogonal design and ANOVA is used to analyse the significance of the electromagnetic parameter data of the TPMLM.

Based on the above analysis, Table 6 summarises the results of the significant effects of the six variables on the three dependent variables. It is intuitively clear from the table that for the TPMLM studied in this paper, the variables that have significant affect all three performance indicators are current density, coil thickness and permanent magnet thickness. The permanent magnet axial length for two performance indicators, and the air gap thickness and coil axial length for only one performance indicator.

TABLE 7 Optimised design variables for TPMLM.

Variable	Unit	Initial value	Values
J_m	A/mm^2	4	[4 , 5 , 6]
h_w	mm	8	[6 , 10 , 14]
h_{pm}	mm	6	[6 , 7.5 , 9]
τ_w	mm	8	[6 , 7 , 8]
τ_{pm}	mm	18	[18 , 24]

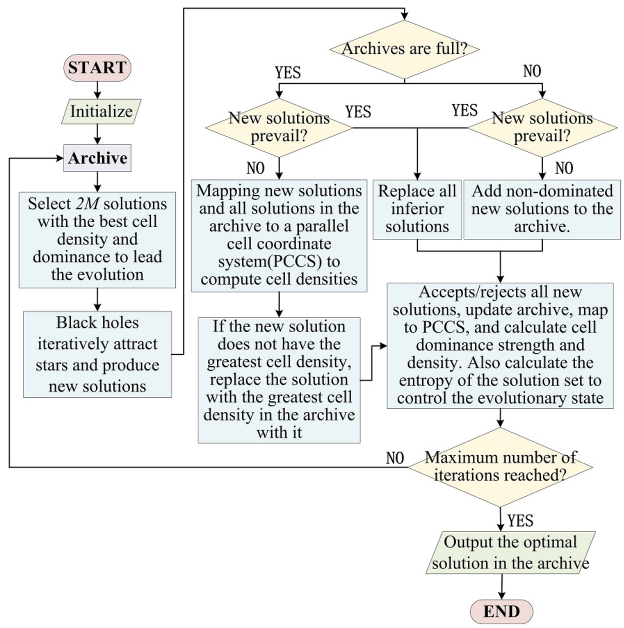

FIGURE 13 AMOBH algorithm flowchart.

Due to the need to control the cost of permanent magnets, five parameters other than air gap thickness are selected as optimal design variables. In addition, to satisfy the actual process constraints, such as the motor outer diameter not exceeding 90 mm and the coil axial length not exceeding 8 mm, the initial values and optimization ranges of the design variables to be optimised are set as shown in Table 7.

4.2 | Motor optimization method based on AMOBH

The adaptive Multi-objective Black Hole Algorithm [19] (AMOBH) is an improved version of the Black Hole Algorithm, which has better performance in terms of convergence performance, population diversity and computational efficiency compared to commonly used multi-objective evolutionary algorithms in dealing with complex high-dimensional problems [22]. Different from the BH algorithm (original single objective version), AMOBH searches the entire space of solutions(stars) and finds the multiple global optimum solutions (Pareto solutions). The flowchart of AMOBH algorithm is shown as Figure 13. Here, the entropy represents the uniformity and diversity of approximate Pareto solutions. Larger entropy means better uniformity and diversity [23].

Firstly, the approximate model of the objective function is constructed using the optimal modelling method proposed in the previous chapter, and the dataset after significance analysis is substituted into it. Then, the parameters of AMOBH, such as the number of inputs and outputs, the size of the population and archive capacity, and the number of iterations, are set to execute the AMOBH optimization algorithm until the Pareto solution set is output. The Pareto frontiers output by AMOBH after reaching the maximum number of iterations are shown in Figure 14. Due to multiple constraints and limited parameter optimization range, the Pareto frontiers are more concentrated in the search space.

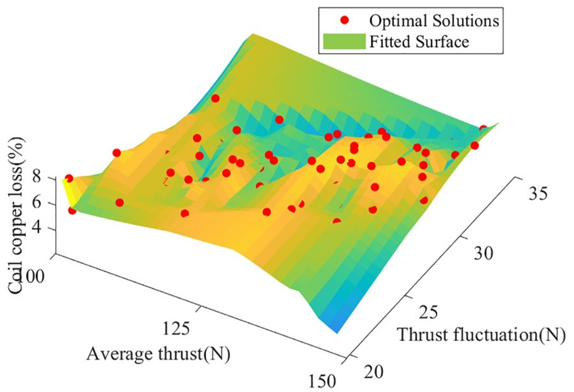

FIGURE 14 Pareto fronts for AMOBH outputs.

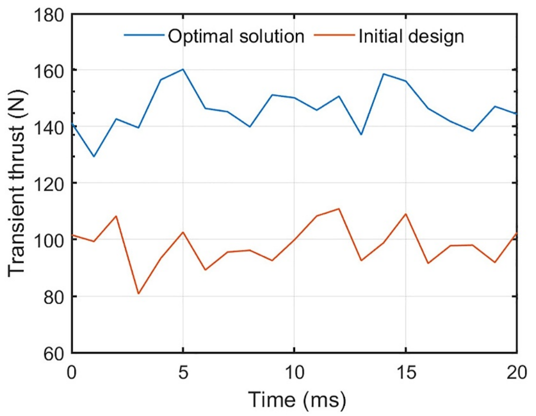

FIGURE 15 Transient thrust comparison.

The Pareto solution sets in Figure 15 satisfy all the constraints in (9), yet further optimization of them is still required. This section highlights three sets of optimised design results with distinctive features are selected in this section, as shown in Table 8.

Based on the Table 8, Design 1 exhibits the highest average thrust (148.35 N) but also the largest permanent magnet volume and notable thrust fluctuations. Conversely, Design 2 boasts the smallest thrust fluctuation (14.99%) and magnet volume, with a competitive average thrust, while Design 3 consumes the least copper in the coils (4.02%) yet lags in both average thrust and thrust stability. Given the primary objective of maximising average thrust for TPMLM, Design one emerges as the primary choice, excluding Design 3. Further analysis reveals Design 1's superiority in coil copper consumption efficiency over Design 2. However, Design 2 marginally prevails in minimising thrust fluctuations and permanent magnet costs. Comprehensively, Design one is deemed the optimal design, balancing key performance metrics and cost considerations. The listed three optimal designs also show that different optimization goals conflict with each other.

Table 9 displays the results of the optimal solution performance calculations for the approximate model and FEA, respectively, which shows that the approximate model constructed in this section can still maintain a very high level of accuracy in the case of insufficient FEA data.

Figure 15 illustrates the comparison between the instantaneous thrust curves of the initial design and the optimal solution output from the FEA. After the multi-objective optimization, the average thrust of the TPMLM has increased by 49.37%, the percentage of thrust fluctuation has

TABLE 8 Comparison of the results of three optimised designs.

Variable	Unit	Initial value	Optimised design 1	Optimised design 2	Optimised design 3
J_m	A/mm^2	4	5.19	4.84	4.05
h_w	mm	8	7.49	7.44	7.39
h_{pm}	mm	6	8.11	7.35	7.89
τ_w	mm	8	6.32	7.22	6.57
τ_{pm}	mm	18	21.51	18.73	19.38
F_{av}	N	97.95	148.35	130.14	101.42
F_{pk}	N	30.10	29.38	21.70	22.97
P_{cua}	W	28.32	30.18	33.8	15.73
P_{cua}%	/	7.96%	5.35%	6.73%	4.02%
F_{pk}%	/	30.73%	18.46%	14.99%	20.39%
V_{pm}	mm^3	19,707	27,507	21,068	23,927

TABLE 9 Comparison of results from approximate models and FEA.

Variable	Approximate model	FEA
$F_{av}/(N)$	148.35	146.31
$F_{pk}/(N)$	29.38	30.93
$P_{cua}/(W)$	30.18	29.59
$P_{cua}\%$	5.35%	5.32%
$F_{pk}\%$	19.8%	21.14%

decreased by 9.59%, and the percentage of copper consumption of the coil has been decreased by 2.64%, but the average value of copper consumption of the coil has been increased by 6.57%. In addition, although the overall motor performance has improved, at the same time the permanent magnet volume has increased by 39.5%. When converted to thrust to volume ratio (N/mm^3), it is 0.00497 before optimization and 0.00532 after optimization, which is an increase of about 7% and is within the acceptable range. In conclusion, the optimal solutions satisfy all the optimization objectives and constraints, and the comparison results with the finite element analysis prove the effectiveness of the multi-objective optimization method.

5 | CONCLUSION

In this paper, an electromagnetic field modelling and optimization method for slotted core TPMLM was proposed. This approach integrates a Bayesian algorithm with an FEA-based DNN model, and adopted a multi-objective black hole algorithm to achieve the optimization of the thrust performance and the reduction of the copper consumption of the coil.

After multi-objective optimization, the average thrust of TPMLM increased by 49.37%, the thrust fluctuation percentage decreased by 9.59%, and the coil copper consumption percentage decreased by 2.64%.

This data-driven model proves to be an efficient and valuable tool for solve electromagnetic field problems. It applies to thermal field analysis and may provide an innovative approach in motor design and optimization in the future.

AUTHOR CONTRIBUTIONS

Tao Wu: Conceptualization; investigation; methodology; writing – original draft; writing – review & editing. **Peipei Dai**: Conceptualization; writing – original draft; writing – review & editing. **Kai Zhu**: Writing – original draft; writing – review & editing. **Yachao Zhu**: Investigation; writing – review & editing.

ACKNOWLEDGEMENT

This research was supported in part by the National Natural Science Foundation of China under grant 2021343163.

Open access publishing facilitated by University of Technology Sydney, as part of the Wiley - University of Technology Sydney agreement via the Council of Australian University Librarians.

CONFLICT OF INTEREST STATEMENT

The authors declare no conflicts of interest.

DATA AVAILABILITY STATEMENT

The data that support the findings of this study are available within the article. Additional data related to the finite element modeling and the deep neural network training process are available from the corresponding author upon reasonable request. The raw data generated and analyzed during the current study are not publicly available due to proprietary restrictions, but are available for inspection by any qualified researcher.

ORCID

Tao Wu https://orcid.org/0000-0002-9066-8455
Peipei Dai https://orcid.org/0009-0006-5592-0746
Yachao Zhu https://orcid.org/0009-0007-4994-0908

REFERENCES

1. Li, K., Zhang, X., Chen, H.: Design optimization of a tubular permanent magnet machine for cryocoolers. IEEE Trans. Magn., 51(5), 1–8 (2014). https://doi.org/10.1109/TMAG.2014.2332437
2. Zhao, S., Liang, J., Zhao, Y.: Research on large thrust cylindrical permanent magnet linear motor for directly driving machine tool spindle. Machine Tool and Hydraulic, 42(09), 66–70 (2014). https://doi.org/10.3969/j.issn.1001-3881.2014.09.018
3. Xuzhen, H., et al.: Calculation and experimental study on temperature rise of a high OverLoad tubular permanent magnet linear motor. IEEE Trans. Plasma Sci. 41(5), 1182–1187 (2013). https://doi.org/10.1109/TPS.2013.2246872
4. Musolino, A., et al.: Optimal design of EMALS based on a double-sided tubular linear induction motor. IEEE Trans. Plasma Sci. 43(5), 1326–1331 (2015). https://doi.org/10.1109/TPS.2015.2413675
5. Wu, T., et al.: Design and analysis of a new down-the-hole electromagnetic hammer driven by tube linear motor. IET Electr. Power Appl. 11(9), 1558–1565 (2017). https://doi.org/10.1049/iet-epa.2017.0208
6. Tan, Q., et al.: Analysis of flux linkage and detent force for a modular tubular permanent magnet synchronous linear motor with large slots. IEEE Trans. Energy Convers. 34(3), 1532–1541 (2019). https://doi.org/10.1109/TEC.2019.2912873
7. Tomczuk, B., Schroder, G., Waindok, A.: Finite-element analysis of the magnetic field and electromechanical parameters calculation for a slotted permanent-magnet tubular linear motor. IEEE Trans. Magn. 43(7), 3229–3236 (2007). https://doi.org/10.1109/TMAG.2007.894216
8. Chen, H., Li, Z., Yan, W.: Flux characteristics analysis of a single-phase tubular permanent magnet linear motor based on 3-d magnetic equivalent circuit. IEEE Trans. Plasma Sci. 47(5), 2309–2315 (2019). https://doi.org/10.1109/TPS.2019.2899930
9. Li, L., et al.: Magnetic field of a tubular linear motor with special permanent magnet. IEEE Trans. Plasma Sci. 39(1), 83–86 (2010). https://doi.org/10.1109/TPS.2010.2057519
10. Wang, X., Wang, Y., Wu, T.: The review of electromagnetic field modeling methods for permanent-magnet linear motors. Energies 15(10), 3595 (2022). https://doi.org/10.3390/en15103595
11. Smith, P.F., Ganesh, S., Liu, P.: A comparison of random forest regression and multiple linear regression for prediction in neuroscience. J. Neurosci. Methods 220(1), 85–91 (2013). https://doi.org/10.1016/j.jneumeth.2013.08.024
12. Keskes, H., Braham, A.: Recursive undecimated wavelet packet transform and DAG SVM for induction motor diagnosis. IEEE Trans. Ind. Inf. 11(5), 1059–1066 (2015). https://doi.org/10.1109/TII.2015.2462315
13. Yang, Y., et al.: Research on structural optimization of coreless permanent magnet synchronous linear motor based on deep neural network model. Journal of China Electrical Engineering 39(20), 6085–6094 (2019). https://doi.org/10.13334/j.0258-8013.pcsee.182019

14. Yan, J., et al.: Multi-objective hierarchical optimization design of cylindrical permanent magnet linear motor with non-uniform teeth for active suspension. Journal of Military Engineering 44(01), 40–50 (2023). https://doi.org/10.12382/bgxb.2022.0756
15. Peng, Z., et al.: Multi-objective optimization of cylindrical permanent magnet linear motor with NSGAII. Comput. Age(01), 21–25 (2023). https://doi.org/10.12677/MOS.2023.123255
16. Coello, C.A.C., Pulido, G.T., Lechuga, M.S.: Handling multiple objectives with particle swarm optimization. IEEE Trans. Evol. Comput. 8(3), 256–279 (2004). https://doi.org/10.1109/TEVC.2004.826067
17. Deb, K., et al.: A fast and elitist multiobjective genetic algorithm: nsga-II. IEEE Trans. Evol. Comput. 6(2), 182–197 (2002). https://doi.org/10.1109/4235.996017
18. Zhang, Q., Li, H.: A multiobjective evolutionary algorithm based on decomposition and probability model. IEEE Trans. Evol. Comput. 1(1), 1–8 (2012). https://doi.org/10.1109/CEC.2012.6252954
19. Wu, T., et al.: Multiobjective optimization of a tubular coreless LPMSM based on adaptive multiobjective black hole algorithm. IEEE Trans. Ind. Electron. 67(5), 3901–3910 (2019). https://doi.org/10.1109/TIE.2019.2916347
20. Lee, D.Y., et al.: A study on the efficiency optimum design of a permanent magnet type linear synchronous motor. IEEE Trans. Magn. 41(5), 1860–1863 (2005). https://doi.org/10.1109/TMAG.2005.846466
21. Sasaki, H., Hidaka, Y., Igarashi, H.: Explainable deep neural network for design of electric motors. IEEE Trans. Magn. 57(6), 1–4 (2021). https://doi.org/10.1109/TMAG.2021.3063141
22. Chong, W., et al.: AMOBH: adaptive multiobjective black hole algorithm. Comput. Intell. Neurosci. 2017, 1–19 (2017). https://doi.org/10.1155/2017/6153951
23. Hu, W., Yen, G.G., Zhang, X.: Multiobjective particle swarm optimization based on Pareto entropy. J. Software 25(5), 1025–1050 (2014). https://doi.org/10.13328/j.cnki.jos.004496

How to cite this article: Wu, T., et al.: Modelling and optimization of TPMLMs with slotted stators based on Bayesian DNN. IET Electr. Power Appl. 18(11), 1679–1689 (2024). https://doi.org/10.1049/elp2.12504